Optics Communications 282 (2009) 3069–3075

Contents lists available at ScienceDirect

Optics Communications

journal homepage: www.elsevier.com/locate/optcom

Polarizing beam splitter of two-layer dielectric rectangular transmission gratings in Littrow mounting

Jiangjun Zheng, Changhe Zhou *, Jijun Feng, Hongchao Cao, Peng Lu

Information Optics Lab, Shanghai Institute of Optics and Fine Mechanics, Chinese Academy of Sciences, P.O. Box 800-211, Shanghai 201800, China

ARTICLE INFO

Article history:
Received 27 November 2008
Received in revised form 28 April 2009
Accepted 7 May 2009

Keywords:
Grating
Beam splitter
Modal method

ABSTRACT

We theoretically investigated the design of polarizing beam splitters (PBS) of two-layer dielectric rectangular transmission gratings in Littrow mounting. The PBS grating is aimed to separate TE and TM polarized waves into two different transmitted orders, i.e. the 0th and −1st orders. The polarization-dependent diffraction process is analyzed by using a simplified modal method. The mode reflection and transmission at the interface of the two layers are illustrated. Design equations are given based on the average mode indices of the even and odd modes inside the grating region, which are verified by using rigorous coupled wave analysis. Moreover, with simulated annealing algorithm, two kinds of two-layer PBS gratings are optimized for operation over the C-band (1520–1570 nm). Compared with the single-layer transmission PBS gratings, such two-layer scheme exhibits a great flexibility of design. The PBSs of two-layer dielectric transmission gratings should be useful for practical applications.

1. Introduction

The polarization control of optical beams is very important in many optical systems. A polarizing beam splitter (PBS) is such an optical element that can separate a beam into two orthogonally polarized beams. It can be widely used in optical information processing systems, such as magneto-optic data storage, free-space optical switching, etc. A birefringent prism or a multilayer dielectric coating [1] can be designed as a PBS. The birefringent prism may be heavy, bulky, expensive and not easily integrated. A multilayer coating also cost much to fabricate. The gratings whose periods are comparable to the incident wavelength can behave very differently for differently polarized waves. A PBS is realizable by optimizing the grating parameters. Compared with the conventional PBSs, the PBS gratings can be cheap, light and compact for effective packaging. During the past decades, several PBS gratings have been designed or fabricated, which can separate TE (electric field vector parallel to the grating groove) and TM (magnetic field vector parallel to the grating groove) polarized beams into its reflected 0th order and transmitted 0th order respectively, such as multilayer dielectric gratings [2], metallic wire-grid gratings [3], sub-wavelength gratings in the quasi-static domain [4], and embedded metal-wire nano-gratings [5]. A PBS grating can also separate the TE and TM polarized beams into the transmitted or reflected 0th and −1st orders in Littrow mounting with both high efficiencies and extinction ratios [6–10]. For the case of dielectric binary transmission gratings, a simplified modal method can describe the diffraction process very accurately [11]. The classic modal method was used to calculate rigorous diffraction efficiencies of gratings by expanding the field inside the grating into a series of discrete modes that can be supported by a corresponding infinite periodic waveguide [12]. In the simplified modal method, only the propagating modes are considered. It has been shown that the simplified modal method can function as a good design guideline for several grating beam splitters [11,13–18]. To our knowledge, no one has ever demonstrated PBSs of two-layer dielectric rectangular transmission gratings in Littrow mounting with a modal analysis to reveal the diffraction process.

In this paper, we theoretically investigated polarization-dependent diffraction of a two-layer dielectric rectangular transmission grating in Littrow mounting. The simplified modal method is used to illustrate the diffraction process in the grating layers. The reflection and transmission of the propagating modes at the interface of the two layers are analyzed. Design equations are then given for separating the TE and TM polarized waves in the transmitted 0th and −1st orders. Diffraction efficiencies are obtained by using rigorous coupled-wave analysis (RCWA) [19], which prove the validity of the design equations. Together with the simulated annealing (SA) algorithm [20,21], PBS gratings can be optimized to function over a wide band with both high diffraction efficiencies and high extinction ratios. Examples of two kinds of two-layer PBS gratings are given for operation over the C-band (1520–1570 nm). In comparison with the single-layer grating, the two-layer grating exhibits great flexibility for the PBS design. The optimized two-layer PBS gratings can achieve better performance than the single-layer PBS

* Corresponding author. Fax: +81 21 69918213.
E-mail address: jzhj01@126.com (C. Zhou).

0030-4018/$ - see front matter © 2009 Elsevier B.V. All rights reserved.
doi:10.1016/j.optcom.2009.05.011

gratings. The description in this paper should help our understanding of the diffraction process, and it will contribute to design various grating beam splitters, polarization dependent or independent, by using the two-layer scheme. This kind of PBS gratings should be interesting in practical applications.

2. Polarization-dependent diffraction behavior

The two-layer transmission grating structure is shown in Fig. 1. A monochromatic plane wave is incident from the cover (air, $n_c = 1$) with angle $\theta_{inc} = \arcsin(\lambda/2d)$; i.e., the Littrow angle, where λ is the incident wavelength in vacuum, and d is the grating period. The transmitted 0th and -1st orders propagates symmetrically in the substrate with angle $\theta_0 = \theta_{-1} = \arcsin(\lambda/2n_s d)$, where n_s is the refractive index of the substrate. The grating region with depth h is assumed to have two layers with the same duty cycle f (ratio of the grating-ridge width to the grating period). The thickness and the refractive index of the ridge of ith layer are h_i and n_i ($i = 1, 2$), respectively. The medium in the groove is air. In this paper, it is aimed to use this kind of transmission grating structure as a PBS, which means the TE and TM polarized components of the incident wave are separated in the two transmitted orders.

Several parameters of the two-layer gratings are kept constant in advance. The incident wave length λ is set to be 1550 nm to allow the designed PBSs to be used in optical communication systems. The substrate is fused silica with $n_s = 1.45$, which is a cheap, most widely-used optical material. The ridge of layer 2 is also fused silica with $n_2 = 1.45$. The ridge of layer 1 has a larger refractive index $n_1 = 2.0$. Since there are several optical materials that have refractive indices around 2.0, such as Ta_2O_5, this two-layer element may be practically fabricated [20]. Then, only the grating geometrical parameters are left to be varying.

The two-layer scheme is more complex than the simple binary ones. Each grating layer will have an impact on the transmission efficiencies. We wonder whether there is any average effect of the two layers. Therefore, we considered the case that the thicknesses ratio of the two grating layers is kept constant. An example is given in Fig. 2, which shows that the -1st-order diffraction efficiencies vary versus the duty cycle f and the total grating depth h with a thickness ratio $h_1/h_2 = 1$ for both TE and TM polarizations. It is obvious that the main features are similar to those of the binary fused-silica gratings in Fig. 2 of Ref. [11]. The locations of the bright stripes are different for TE and TM polarizations. Especially,

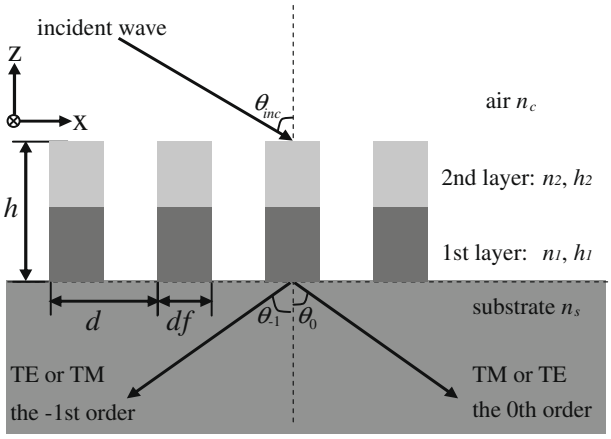

Fig. 1. Schematic of a two-layer dielectric transmission grating PBS: n_c and n_s, refractive indices of air and substrate, respectively; d, grating period; h, grating depth; f, grating duty cycle; h_i and n_i, thickness and refractive index of the grating ridge of the ith layer ($i = 1, 2$), respectively; θ_{inc}, incident angle; θ_0 and θ_{-1}, diffraction angles of the 0th and -1st orders in substrate, respectively.

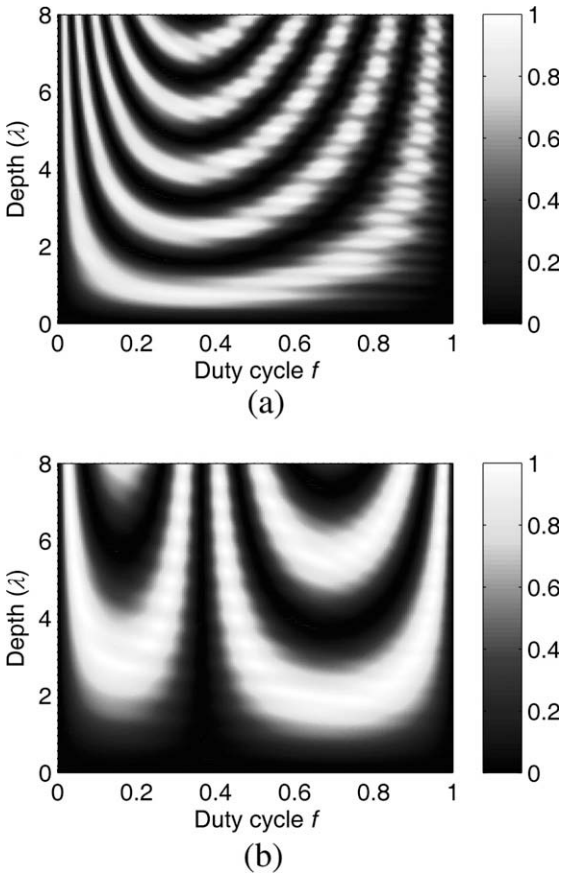

Fig. 2. 1st-order diffraction efficiency versus the duty cycle f and the total grating depth h: (a) TE polarization and (b) TM polarization. The period d of the two-layer grating is 880 nm, the thicknesses ratio h_1/h_2 is 1, and the incident wavelength λ is 1550 nm.

there is a dark stripe which is almost straight and independent of the grating depth around the duty cycle $f = 0.36$ in Fig. 2b for TM polarization. It is interesting that a two-layer grating has such depth-independent behavior, which means that a polarizer or PBS can also be designed by using such a two-layer scheme just like by using a binary phase grating [11,15]. Fig. 2 suggests an average effect of the two-grating layers, which is shown by the similar diffraction patterns as the binary gratings.

Much work has been done on the analysis of binary phase beam splitter gratings with a simplified modal method [9,11,13–18]. In the simplified modal method, the effective grating mode indices, mode profiles and overlap integrals are intensively concerned [22]. The effective mode indices are proportional to modes propagation constants along the grating grooves and ridges, which are determined by the dispersion equation

$$F(n_{eff}^2) = \cos(k_r f d)\cos(k_g(1-f)d) - \frac{k_r^2 + k_g^2}{2k_g k_r}\sin(k_r f d)\sin(k_g(1-f)d) = \cos(k_x d) \quad (1a)$$

$$F(n_{eff}^2) = \cos(k_r f d)\cos(k_g(1-f)d) - \frac{n_g^4 k_r^2 + n_r^4 k_g^2}{2n_g^2 n_g^2 k_g k_r}\sin(k_r f d) \times \sin(k_g(1-f)d) = \cos(k_x d) \quad (1b)$$

with

$$K_x = \frac{2n_c\pi}{\lambda}\sin\theta_{inc}, \quad k_r = \frac{2\pi}{\lambda}\sqrt{n_r^2 = n_{eff}^2}, \quad K_g = \frac{2\pi}{\lambda}\sqrt{n_g^2 - n_{eff}^2}$$

where n_r is the refractive index of the grating ridge, n_g is that of the grating groove, n_{eff} is the effective mode index, the mode propagation constant k_z is $2n_{eff}/\lambda$, Eq. (1a) is for TE polarization and Eq. (1b) is for TM polarization.

For a deep low-contrast binary phase grating in Littrow mounting ($\cos(k_x d) = -1$), a two-beam-interference view [11] is employed to reveal the polarization-dependent diffraction process. The reflections at the grating interfaces and the evanescent grating modes are neglected. By assuming equal excitations of the only two propagating grating modes, the transmitted −1st-order efficiency η_{-1} was shown to be [11,22]:

$$\eta_{-1}(h) = \sin^2\left(\frac{\pi(n_{0eff} - n_{1eff})h}{\lambda}\right) \tag{2}$$

where n_{0eff} and n_{1eff} ($n_{0eff} \geqslant n_{1eff}$) are the effective indices of mode 0 and mode 1, respectively. The sinusoidal efficiency curves versus the grating depth coincide with the main features of the curves of rigorous numerical results [11].

For the two-layer scheme in Fig. 1, it is necessary to know the mode properties in each layer. Fig. 3 shows the mode index differences ($n_{0eff} - n_{1eff}$) versus the duty cycle f for both TE and TM polarizations for the two-layer structure used in Fig. 2. The maximum index differences for $n_r = 2.0$ are over twice of those for $n_r = 1.45$ with the same polarization state. From Eq. (2), it is easily known that a higher refractive index of the grating ridge can result in a smaller depth to achieve the maximum −1st-order efficiency. It is also shown in Fig. 3 that a point with $n_{0eff} = n_{1eff}$ is observed only for TM polarization with $0 < f < 1$ for both $n_r = 1.45$ and $n_r = 2.0$. It can be called the special point which is related to a (f, d) pair. The special point has been investigated in detail for single-layer fused-silica gratings [11] with a depth-independent diffraction for TM wave according to Eq. (2). Here, the duty cycles of the special points of the two layers are different for the same period. However, there is still a straight dark stripe in Fig. 2b with duty cycle $f = 0.36$. There, the mode index differences ($n_{0eff} - n_{1eff}$) are equal in the two layers as shown in Fig. 3. The reason for such depth-independent diffraction lies in the parity of the grating modes.

Fig. 4 shows the x-dependent mode profiles of amplitude E_y for TE polarization and H_y for TM polarization. In this paper, the modes which are even-symmetric in the grating ridge are called "even modes", and the modes which are odd-symmetric in the grating ridge are called "odd modes". In Fig. 4a, mode 0 is even and mode 1 is odd for both grating layers for TE polarization. While for TM polarization, mode 0 is even for $n_r = 2.0$, while it is odd for $n_r = 1.45$; the contrary situation comes for mode 1. By using the

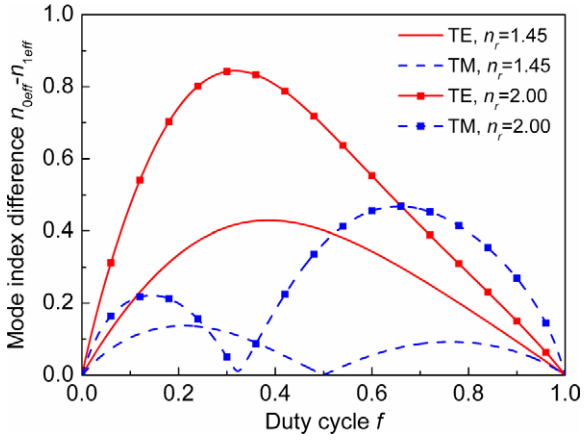

Fig. 3. Mode index difference ($n_{0eff} - n_{1eff}$) of the two propagating grating modes (mode 0 and mode 1) versus the duty cycle f for grating with period $d = 880$ nm. The incident wavelength λ is 1550 nm.

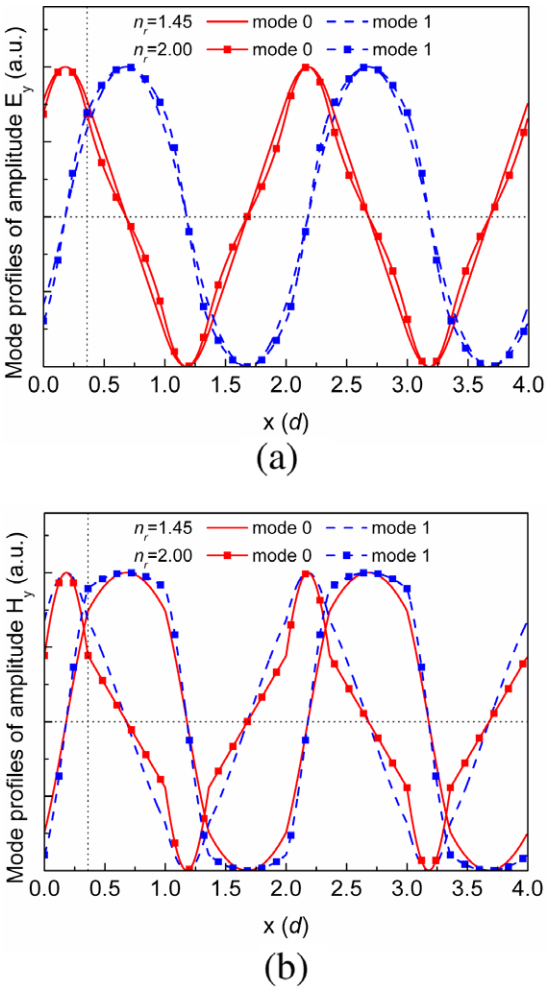

Fig. 4. Mode profiles of x-dependent amplitude for grating with period $d = 880$ nm and duty cycle $f = 0.36$: (a) E_y for TE modes and (b) H_y for TM modes. The dotted vertical line indicates the duty cycle 0.36, and the horizontal dotted line indicates the line of $E_y = 0$ and $H_y = 0$. The incident wavelength λ is 1550 nm.

overlap integrals [22], it is easily shown that an even/odd mode can only exchange energy with an even/odd mode. There is no coupling between an even mode and an odd mode. It is better to use the expressions of "even mode" and "odd mode" rather than "mode 0" and "mode 1". Although the mode profiles for TM wave in Fig. 4 are not as smooth and similar to the sinusoidal curve as those for TE wave, which is due to the different boundary conditions at the edges of the grating ridge, the two TM modes are still almost equally excited by the incident wave, just as the two TE modes. The evanescent high order modes are weakly excited because their spatial frequencies are higher than the incident wave.

At the interface of the two grating layers, the reflection and transmission of the propagating modes can be analyzed by matching the boundary condition of the electromagnetic fields. The fields in the two layers can be written in a modal basis as:

$$\Phi_I(x,z) = \sum_p \left[a^+_{I,p} u_{I,p}(x) \exp(ik'_{I,p} z) + a^-_{I,p} u_{I,p}(x) \exp(-ik'_{I,p} z)\right] \tag{3a}$$

$$\Phi_{II}(x,z) = \sum_p \left[a^+_{II,p} u_{II,p}(x) \exp(ik'_{II,p} z) + a^-_{II,p} u_{II,p}(x) \exp(-ik'_{II,p} z)\right] \tag{3b}$$

where I and II denotes the first and second grating layers, $u_{i,p}(x)$ is the pth normalized mode [22] in the ith layer, $a^+_{i,p}$ and $a^-_{i,p}$ are mode coefficients, whose relationship can be expressed as:

$$\begin{bmatrix} a_{I,p}^{-} \\ a_{II,p}^{+} \end{bmatrix} = \begin{bmatrix} r_{11} & t_{21} \\ t_{12} & r_{22} \end{bmatrix} \begin{bmatrix} a_{I,p}^{+} \\ a_{II,p}^{-} \end{bmatrix} \tag{4}$$

where r_{11} is the reflection matrix for the modes in the first layer, while r_{22} is for the modes in the second layer, and t_{21} is the transmission matrix for modes in the second layer to modes in the first layer, while t_{12} is for modes in the first layer to modes in the second layer. After applying the boundary condition at the interface of the two grating layers, the mode transmission and reflection coefficients for the example two-layer grating can be obtained in Table 1. For reflection, the nonzero values of $|r_{aa}(i,i)|^2$ can be viewed as the reflection efficiency of the ith mode to itself in layer a. In Table 1, the maximum reflection efficiency is $|r_{11}(1,1)|^2$ for TE wave, which is about 4.88%. Therefore, the energy of the incident mode is mostly transmitted, which can also be shown by the nonzero values of t_{12} and t_{21}. $t_{ab}(i,j)$ means the transmission amplitude of the normalized mode j in layer a to the mode i in layer b. However, the related transmission efficiency is not $|t_{ab}(i,j)|^2$. In theory, the transmission efficiency can be written as $t_{ab}(i,j)t_{ba}^{*}(j,i)$, where the superscript * means the complex conjugate. Then, the minimum transmission efficiency in Table 1 is $t_{12}(1,1)t_{21}^{*}(1,1)$, which is about 95.12%. It is the same as $1-|r_{11}(1,1)|^2$, which means the energy conservation is maintained. In this view, although there are transmission amplitudes larger than 1, these transmission efficiencies are very close to, but still less than 1. Considering the mode symmetry in Fig. 4, the zero values in Table 1 clearly show that there is no reflection or transmission coupling between an even/odd mode and an odd/even mode in the two grating layers. The modes in the first layer can transfer most energy to the modes with the same symmetry in the second layer. Further more, the phases of the nonzero values of t_{12} and t_{21} are no more than 1.7°, which is very small. These phase changes can be neglected for deep gratings.

Based on the above illustration of mode couplings, in the two-beam-interference view [11], the diffraction efficiency of η_{-1} for the structure in Fig. 1 can be expressed by

$$\eta_{-1}(h) = \sin^2\left(\frac{\pi(\bar{n}_{even}-\bar{n}_{odd})h}{\lambda}\right) = \sin^2\left(\frac{\pi\Delta\bar{n}_{eff}h}{\lambda}\right) \tag{5}$$

with

$$\begin{aligned} &\Delta\bar{n}_{eff} = (\Delta n_{1,eff}h_1 + \Delta n_{2,eff}h_2)/h, \Delta n_{1,eff} = n_{i,even} - n_{i,odd}, \\ &\bar{n}_{even} = (n_{1,even}h_1 + n_{2,even}h_2)/h, \bar{n}_{odd} = (n_{1,odd}h_1 + n_{2,odd}h_2)/h. \end{aligned} \tag{6}$$

where $n_{i,even}$ and $n_{i,odd}$ are the even-mode index and odd-mode index of the ith grating layer (i = 1, 2); respectively; $\bar{n}_{even}$ and $\bar{n}_{odd}$ are the average index of the even modes and odd modes, respectively; $\Delta n_{i,eff}$ is index difference of the ith grating layer, and the $\Delta\bar{n}_{eff}$ is the average index difference. Fig. 4 shows that the $\Delta n_{i,eff}^{TM}$ can be either positive or negative, while $\Delta n_{i,eff}^{Te}$ is always positive.

With Eqs. (5) and (6), the main features of Fig. 2 can be well explained for both the TE and TM polarizations. Fig. 5 shows the transmission efficiencies versus grating depth for the grating in Fig. 2 with f = 0.36, which indicates the center of straight dark stripe in Fig. 2b. As can be seen, the curve of η_{-1}^{TE} is close to the grey sinusoidal curve by using Eq. (5). η_{-1}^{TM} is always close to 0 because $\Delta n_{1,eff}^{TM} = -\Delta n_{2,eff}^{TM}$, and almost all the transmitted energy of TM wave is in the 0th order. Numerical results also show that the period of the fluctuations in curve of η_0^{TM} is about $\lambda/2\bar{n}_{even}$ (or $\lambda/2\bar{n}_{odd}$, about 925 nm), which is due to reflections of the two modes at the air-grating and grating-substrate interfaces [11]. Fig. 5 shows that the concept of the average mode index can be applicable for the two-layer grating in Fig. 1. In the following section, we will show a rough design method directly based on the above modal analysis.

3. Design of PBSs

For a PBS, the extinction ratio are key important, which can be defined as

$$C = \min\{C_o, C_{-1}\} \tag{7}$$

with

$$C_0 = -10\log\left(\eta_0^{Ta}/\eta_0^{Tb}\right), \quad C_{-1} = -10\log\left(\eta_{-1}^{Tb}/\eta_{-1}^{Ta}\right). \tag{8}$$

where superscripts Ta and Tb can be either TE and TM or TM and TE, respectively; η_0 and η_{-1} are the transmission efficiencies in the 0th and −1st orders, respectively; C_0 and C_{-1} are the extinction ratios of the 0th-order and −1st-order transmissions in the unit of dB, respectively. The PBS is designed to produce pure Ta wave in the −1st order and Tb wave in the 0th order. For the transmission grating structure in Fig. 1, since the incident energy is mainly redistributed in the two transmitted orders, when η_o^{Ta} and η_{-1}^{Tb} are very low, η_{-1}^{Ta} and η_0^{Tb} will be high, and then high extinction ratio C can be obtained. From Eq. (5), the design condition for a PBS grating can be expressed by

$$\Delta n_{1,eff}^{Ta}h_1 + \Delta n_{2,eff}^{Ta}h_2 = (2m+1)\lambda/2, \Delta n_{1,eff}^{Tb}h_1 + \Delta n_{2,eff}^{Tb}h_2 = n\lambda \tag{9}$$

where m and n are integers. As is shown in Section 2, $\Delta n_{i,eff}^{TE}$ is always positive, while $\Delta n_{i,eff}^{TM}$ could be negative, zero or positive, because $\Delta n_{i,even}^{TM}$ in each grating layer can be smaller than, equal to, or larger than $\Delta n_{i,odd}^{TM}$. It is necessary to know which case is taking place. It can be made clear by cutting the (f,d) plane into different regions.

Fig. 6 shows the (f,d) curves of the special point with $n_{0eff} = n_{1eff}$ for TM polarization in each grating layer. There are also four dotted lines. It is relatively easy to fabricate gratings with duty cycle $0.3 \leqslant f \leqslant 0.7$, which is located between the two horizontal dotted lines. The condition of $\lambda/2\min(n_i, n_c, n_s) < d < 3\lambda/2\max(n_i, n_c, n_s)$, which are indicated by the two vertical lines, is strong enough to make sure that only two propagating modes/orders exist in the two-layer structure of Fig. 1. Therefore, the center box region is of our interest with $0.3 \leqslant f \leqslant 0.7$ and $\lambda/2\min(n_i, n_c, n_s) < d < 3\lambda/2\max(n_i, n_c, n_s)$. This region is divided into three parts by the (f,d) curves of the special point of each layer, which are labeled by 1, 2, and 3. From Section 2, it can be known that $\Delta n_{i,eff}^{TM}$ is zero on

Table 1
Mode reflection and transmission coefficients at the interface of the two layers of the grating with d = 880 nm, f = 0.36, n_1 = 2.0, n_2 = 1.45. The wavelength λ is 1550 nm. t_{ab} and (i,j) together means the transmission coefficients of mode j in layer a to mode i in layer b, while r_{aa} and (i,j) together means reflection coefficients of mode j to mode i in layer a. Mode 1 and mode 2 are either even- or odd-symmetric as are shown in Fig. 4.

		(1, 1)	(1, 2)	(2, 1)	(2, 2)
TE	r_{11}	0.2209–0.0066i	0	0	0.1208–0.0058i
	r_{22}	−0.2209–0.0051i	0	0	−0.1209–0.0047i
	t_{12}	1.2210–0.0041i	0	0	1.1210–0.0051i
	t_{21}	0.7790–0.0026i	0	0	0.8790–0.0040i
TM	r_{11}	0.0127–0.0302i	0	0	0.0711–0.0039i
	r_{22}	−0.0711–0.0035i	0	0	−0.0143–0.0295i
	t_{12}	0	1.0894–0.0032i	1.2156–0.0341i	0
	t_{21}	0	0.8211–0.0230i	0.9133–0.0027i	0

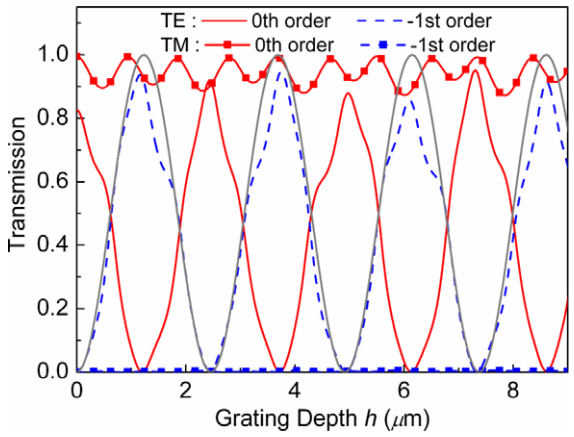

Fig. 5. Transmission efficiency versus the grating depth for both TE and TM polarizations for the grating with period $d = 880$ nm, $f = 0.36$. The two grating layers are of equal thickness. The gray solid line is the sinusoidal curve of Eq. (5) for TE polarization.

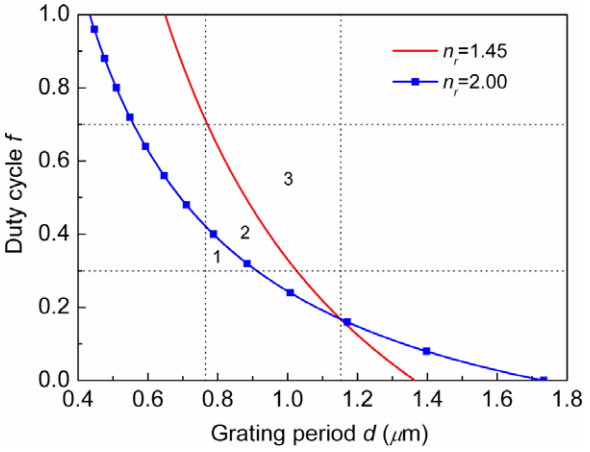

Fig. 6. Illustration of the regions by using (f, d) curves with $n_{0eff} = n_{1eff}$ for TM polarization for each layer of the two-layer grating. Between the horizontal dotted lines is the region with $0.3 < f < 0.7$; between the vertical dotted lines is the region with $\lambda/2\min(n_i, n_c, n_s) < d < 3\lambda/2\max(n_i, n_c, n_s)$. The (f, d) curves cut the center rectangular region into three regions which are labeled by 1, 2, 3. The incident wavelength is 1550 nm.

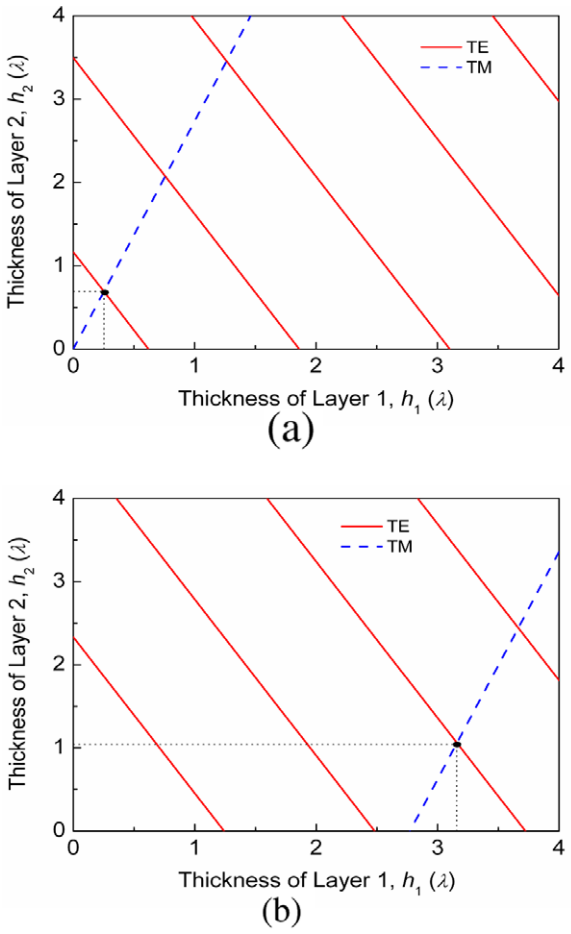

Fig. 7. Lines of the design equation (Eq. (9)) for the grating with period $d = 880$ nm and duty cycle $f = 0.4$. Red solid lines are for TE polarization, and blue dashed lines are for TM polarization. The black point indicates the design location of a PBS.

the (f, d) curve, negative in the downside, and positive in the upside. So, in region 1, the average index difference $\Delta\bar{n}_{eff}^{TM}$ is always negative, while in region 3, it is always positive. In region 2, because $\Delta n_{1,eff}^{TM}$ is positive while $\Delta n_{2,eff}^{TM}$ is negative, $\Delta\bar{n}_{eff}^{TM}$ is a compensated result of the two layers. By choosing proper ratio of the thicknesses of the two grating layers, $\Delta\bar{n}_{eff}^{TM}$ could be zero as the case of Fig. 5. Fig. 6 shows the design flexibility of a two-layer scheme over the binary phase gratings: A two-layer PBS grating design can fall in all the three regions, while one has to follow a special curve of (f, d) to find a lamellar PBS grating.

To prove the validity of Eq. (9), Fig. 7 shows a series of lines by using it for a two-layer grating with $d = 880$ nm and $f = 0.4$ in region 2 of Fig. 6. Fig. 7a is for design of PBS with TM in the 0th order and TE in the −1st order, and Fig. 7b for the opposite case. The intersection points of the TE and TM lines indicate the design parameters of PBSs. For example, at the marked point ($h_1 = 0.253\lambda = 392$ nm, $h_2 = 0.6916\lambda = 1072$ nm) in Fig. 7a, the diffraction efficiency η_0^{TE} and η_{-1}^{TM} are less than 0.35%, η_{-1}^{TE} and η_0^{TM} are more than 88%, and the overall Extinction ratio C is >24 dB. The marked point ($h_1 = 3.16\lambda = 4896$ nm, $h_2 = 1.06\lambda = 1642$ nm) in Fig. 7b produces $\min(\eta_0^{TE}, \eta_{-1}^{TM}) > 84.9\%, \max(\eta_{-1}^{TE}, \eta_0^{TM}) < 0.2\%$, and $C > 26$ dB. This grating is very deep to fabricate. That is because $\Delta\bar{n}_{eff}^{TM}$ is small in region 2. In the next section, we will show a shallower PBS grating in region 3 of Fig. 6 with a much larger $\Delta\bar{n}_{eff}^{Tm}$. Fig. 7 shows Eq. (9) successfully designed PBS gratings for operation at 1550 nm.

4. Optimized PBSs for operation over C-band

It will be convenient if a PBS can exhibit high diffraction efficiency and extinction ratios over a band. Although rough PBS designs for operation at a single wavelength can be directly obtained by using Eq. (9), not all the designs are as good as the single-layer rectangular PBSs ever designed [9,11]. A two-layer transmission grating in Fig. 1 has more geometrical parameters (h_i, n_i, d, f). It has the potential to achieve better performance. Here, the well-known optimization method of SA algorithm is used [20,21]. The aim is to find a two-layer PBS grating for operation over the C-band (1520–1570 nm). The total grating depth h is kept less than 3 μm. The duty cycle f and period d are confined as in Fig. 6.

Fig. 8 shows the diffraction efficiencies and extinction ratios of an optimized PBS with TM wave in the 0th order and TE wave in the −1st order. The grating period d is 1014 nm, and the duty cycle f is 0.3, which lies on the edge of the region 2 in Fig. 6. The layer thicknesses of h_1 and h_2 are 81 nm and 1986 nm, respectively. The total grating depth h is about 2 μm. As is shown, over the wavelength range of 1480–1620 nm, the diffraction efficiency η_{-1}^{TE} is >92% and η_0^{TM} is >95%, the extinction ratio C_0 is >18 dB, and C_{-1}

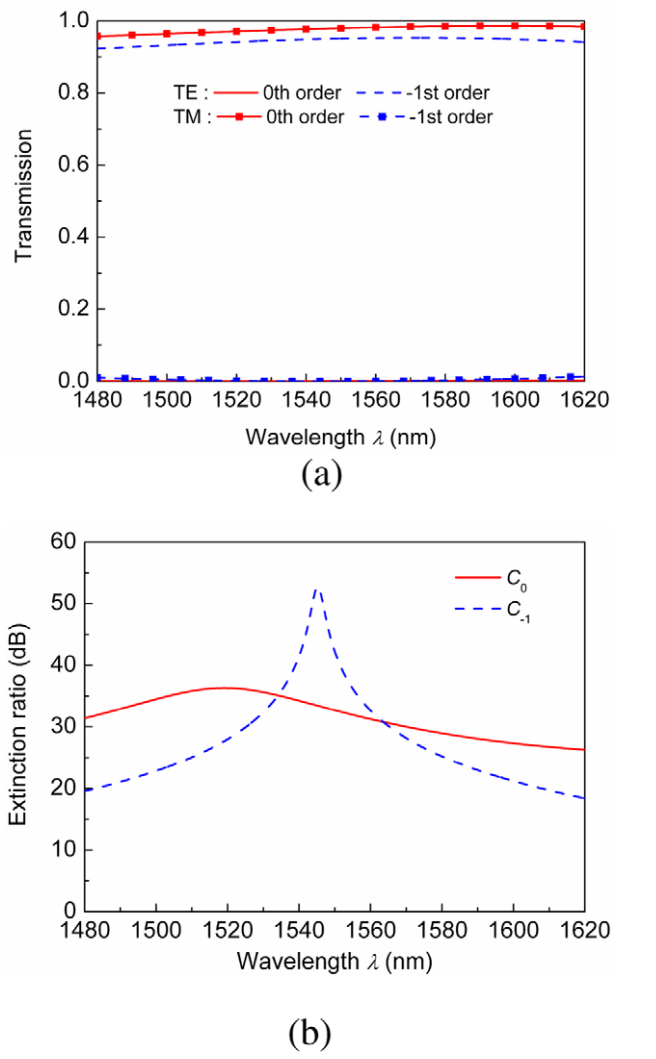

Fig. 8. Diffraction efficiency (a) and extinction ratio (b) versus the incident wavelength in Littrow mounting for the PBS grating for TM wave in the 0th order and TE wave in the −1st order with period $d = 1014$ nm, $f = 0.3$, $h_1 = 81$ nm, $h_2 = 1986$ nm, $n_1 = 2.0$ and $n_2 = 1.45$.

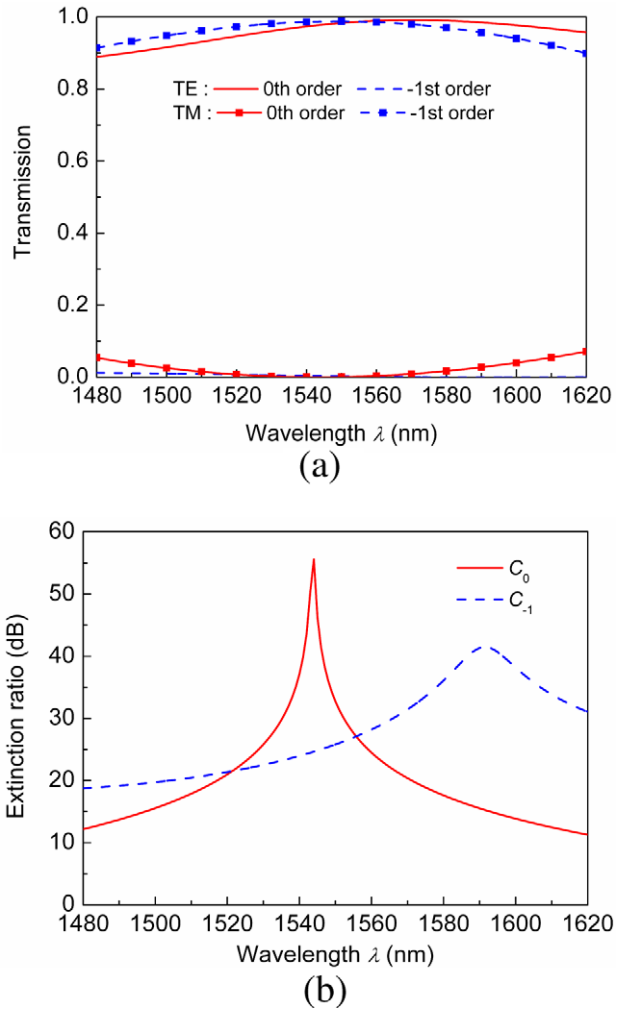

Fig. 9. Diffraction efficiency (a) and extinction ratio (b) versus the incident wavelength in Littrow mounting for the PBS grating for the TM wave in the −1st order and TE wave in the 0th order with period $d = 944$ nm, $f = 0.47$, $h_1 = 1973$ nm, $h_2 = 461$ nm, $n_1 = 2.0$ and $n_2 = 1.45$.

is >26 dB. The grating can function as a highly efficient PBS with high extinction ratios C (>27 dB) over the C-band. This grating can achieves better performances than the binary fused-silica PBS grating in Ref. [9] theoretically.

Fig. 9 shows the diffraction efficiencies and extinction ratios for a PBS with TM wave in the −1st order and TE wave in the 0th order. The (d, f) d is (944 nm, 0.47), which lies in the region 3 in Fig. 6. The thickness of h_1 and h_2 are 1973 nm and 461 nm, respectively. The total grating depth h is about 2.4 μm, which is much smaller than that of the marked point in Fig. 7b. In the C-band, η_0^{TE} is >94%, η_{-1}^{TM} is >97%, and the extinction ratio C is over 20 dB. As η_{-1}^{TE} is small over a relatively wide band (1480–1620 nm), almost pure TM wave can be obtained in the −1st order with a high efficiency.

The above two PBS gratings satisfy the design equation of Eq. (9) approximately as is shown in Table. 2. Only small deviations are caused by the reflection effects. The performance of the designed grating is rather good. It is worth mention that the diffraction pattern in Fig. 9b can not be easily achieved by using a binary fused-silica grating, because the depth will be large. Moreover, by using the two-layer scheme, the grating parameters, other than the geometrical ones, can also be optimized for theoretical analysis [20].

5. Discussions and conclusion

In the modal analysis, the reflections between the layer interfaces are neglected. That is because the index contrast of the materials used in the grating is low. At the grating interfaces, most of the incident energy can be transmitted. The main features of Fig. 2 can be explained by Eq. (5), and the numerically optimized PBS designs satisfy Eq. (9) roughly. However, one should take care to explain all the diffraction behaviors of any two-layer grating in Fig. 1. For example, in Fig. 2a, when the duty cycle approaches 1, the fluctuations of the efficiency seem to increase. That might be

Table 2
Average indices and phases of the two PBS gratings optimized by using the SA. The wavelength λ is 1550 nm. m and n indicate the m and n in Eq. (7).

	h_1 (nm)	h_2 (nm)	$\Delta\bar{n}_{eff}^{TM}$	$\Delta\bar{n}_{eff}^{TE}$	$2\pi\Delta\bar{n}_{eff}^{TM}h/\lambda$	$2pi\Delta\bar{n}_{eff}^{TE}h/\lambda$	m, n
PBS1	81	1986	−0.00157	0.36993	−0.00131	3.09962	$m \approx 0$, $n \approx 0$
PBS2	1973	461	0.32250	0.63731	3.18197	6.28811	$m \approx 0$, $n \approx 1$

because the cheap fused-silica is selected as the substrate material while a grating layer contains a material with a higher refractive index. The effective indices of that layer can be larger than that of the substrate ($n_s \cos\theta_0$) when the duty cycle gets large enough. For such cases, the multiple reflections inside the grating should be considered, just as the case of high-contrast gratings [17,23]. If the substrate has the largest refractive index, the fluctuations could be less. In this paper, the grating PBSs with $0.3 \leqslant f \leqslant 0.7$ and $h \leqslant 3$ μm are preferred for the ease of fabrication. The fluctuations in that region of Fig. 2 are tolerable.

In summary, we theoretically investigated the polarization-dependent diffraction behavior of a two-layer dielectric rectangular transmission grating in Littrow mounting. By the simplified modal method, the diffraction process is revealed. The mode reflection and transmission at the interface of the two layers are analyzed. The design equation of the two-layer PBS gratings is derived, which is an extension of the design equation of a single-layer PBS grating. Numerical results with RCWA are given for the examples of two-layer gratings, which are in accordance with the design method. Because there are more grating parameters, a PBS can be designed more freely. For example, if the grating period d and the duty cycle f are fixed, a PBS grating can be obtained by changing the thickness ratio among grating layers. With the well-known optimization technique of SA algorithm, PBS gratings with excellent performance may be obtained. Two different types of two-layer PBS grating are optimized to be highly efficient over the C-band. The optimized two-layer gratings can probably exhibit better performance than the single-layer gratings [24]. The fabrication example of deep two-layer grating has been reported [20]. Similar simplified modal analysis can also be made for the polarization-independent diffraction of the two-layer grating [20]. The description of the two-layer scheme in this paper may be viewed as a step towards the modal analysis of multilayer transmission gratings. The two-layer PBS grating should also be useful in practical applications.

Acknowledgements

The authors acknowledge the support of National Natural foundation of China (60878035) and Shanghai Science and Technology Committee (07SA14).

References

[1] L. Li, J.A. Dobrowolski, Appl. Opt. 39 (2000) 2753.
[2] R. Tyan, P. Sun, A. Scherer, Y. Fainman, Opt. Lett. 21 (1996) 761.
[3] H. Tamada, T. Doumuki, T. Yamaguchi, S. Matsumoto, Opt. Lett. 22 (1997) 419.
[4] D. Yi, Y. Yan, H. Liu, S. Lu, G. Jin, Opt. Lett. 29 (2004) 754.
[5] L. Zhou, W. Liu, Opt. Lett. 30 (2005) 1434.
[6] S. Habraken, O. Michaux, Y. Renotte, Y. Lion, Opt. Lett. 20 (2005) 2348.
[7] Ph. Lalanne, J. Hazart, P. Chavel, E. Cambril, H. Launois, J. Opt. A 1 (1999) 215.
[8] C.R.A. Lima, L.L. Soares, L. Cescato, Opt. Lett. 22 (1997) 203.
[9] B. Wang, C. Zhou, S. Wang, J. Feng, Opt. Lett. 32 (2007) 1299.
[10] J. Zheng, C. Zhou, J. Feng, B. Wang, Opt. Lett. 33 (2008) 1554.
[11] T. Clausnitzer, T. Kämpfe, E.-B. Kley, A. Tünnermann, A. Tishchenko, O. Parriaux, Appl. Opt. 46 (2007) 819.
[12] L.C. Botten, M.S. CraiG, R.C. Mcphedran, J.L. Adams, J.R. Andrewartha, Opt. Acta 28 (1981) 413.
[13] J. Zheng, C. Zhou, B. Wang, J. Feng, J. Opt. Soc. Am. A 25 (2008) 1075.
[14] T. Clausnitzer, T. Kämpfe, E.-B. Kley, A. Tünnermann, A. Tishchenko, O. Parriaux, Opt. Expr. 16 (2008) 5577.
[15] B. Wang, C. Zhou, J. Feng, H. Ru, J. Zheng, Appl. Opt. 47 (2008) 400.
[16] J. Feng, C. Zhou, J. Zheng, B. Wang, Opt. Commun. 281 (2008) 5298.
[17] E. Gamet, A.V. Tishchenko, O. Parriaux, Appl. Opt. 46 (2007) 6719.
[18] J. Zheng, C. Zhou, J. Feng, H. Cao, P. Lu, J. Opt. A: Pure Appl. Opt. 11 (2009) 015710.
[19] M.G. Moharam, D.A. Pommet, E.B. Grann, T.K. Gaylord, J. Opt. Soc. Am. A 12 (1995) 1077.
[20] M. Shiozaki, M. Shigehara, SEI Technol. Rev. 59 (2005) 27.
[21] B. Goffe, G. Ferrier, J. Rogers, J. Econometrics 60 (1994) 65.
[22] A.V. Tishchenko, Opt. Quantum Electron. 37 (2005) 309.
[23] Ph. Lalanne, J.P. Hugonin, P. Chavel, J. Lightwave Technol. 24 (2006) 2442.
[24] H. Rathgen, H.L. Offerhaus, arxiv:/0809.5242v1 [physics.optics] 30 Sep. 2008.